Surface and deep deformation of the Alps from geodetic and seismic anisotropy measurements

EGU2016-7756 @ TS6.2/GD6.6/SM6.16

X2.206

Salimbeni S.[1], Serpelloni E.[2], Pondrelli S.[1]

1 - Istituto Nazionale di Geofisica e Vulcanologia - Sez. Bologna (Italy)
2 - Istituto Nazionale di Geofisica e Vulcanologia - Centro Nazionale Terremoti (Italy)

ABSTRACT

We study crustal and mantle deformation of the great Alpine area as obtained by Global Position System (GPS) and seismic anisotropy measurements. We derive a new three-dimensional GPS velocity field, obtained from the analysis of thousands of continuous sites operating in the European plate. Using a multi-scale approach we estimate a continuous geodetic strain-rate field, which is compared with the tectonic deformation obtained from the analysis of earthquake focal mechanisms. Deformation of the mantle is inferred from the SKS splitting measurements collected during several experiments and available from different databases. The shear directions (or no-length-change directions) from the geodetic strain-rate field, are compared with the directions of a smoothed map of the SKS orientation over the study area. In this contribution, dynamics and interconnections between crust and mantle are showed and the geodynamic implications are discussed.

SEISMOTECTONICS

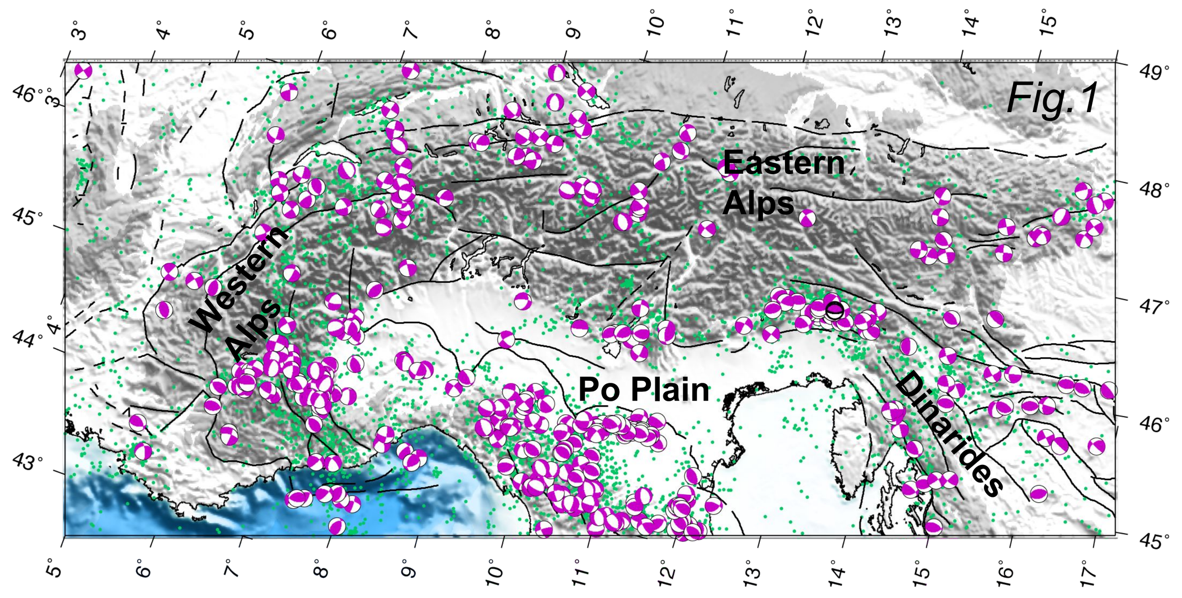

*Seismicity along the Alps and Northern Apennines is mapped in Fig. 1 using data from ISC (green dots, M>=2.5) and focal mechanisms from the CMT and RCMT catalogs and the ETH and EMMA datasets. In the Alps major seismicity occurs in the eastern part, hit by the greatest earthquake of the region, the May 6th, 1976 M6.4 event (**bold** focal mechanism). The highest seismicity rate is present along the active eastern southern Alps thrust front, changing to strike-slip faulting in the Dinarides. In the Western Alps seismicity has lower energy release and different focal mechanisms, with prevailing extensional ones. In the central Alps the poorer seismicity is represented by few thrust events along the boundary belt-Po Plain. In the southern, Po Plain thrust seismicity shows that the outer part of Apennines is active as it is the chain itself, where extension dominates.*

GPS DATA AND 3D VELOCITIES

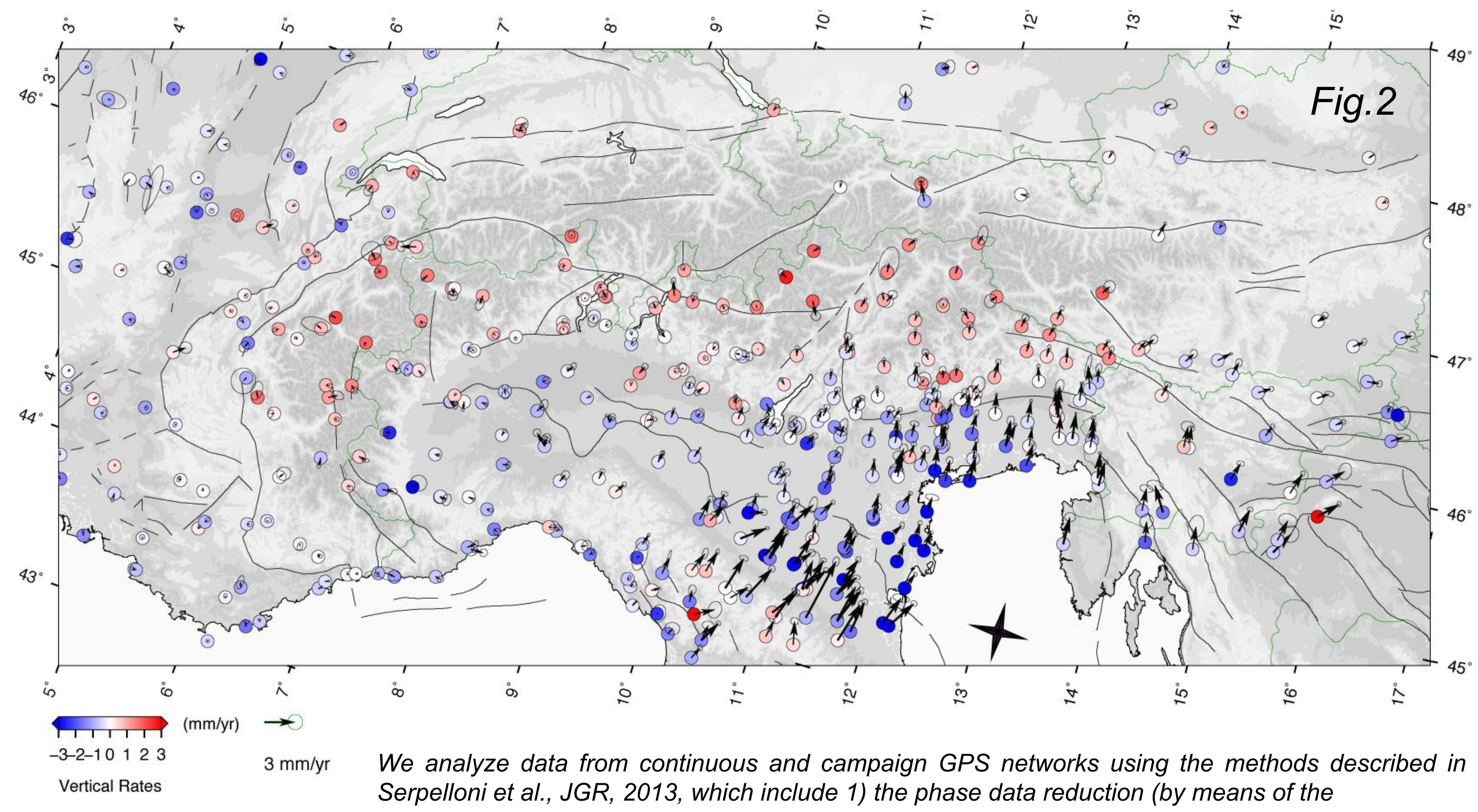

We analyze data from continuous and campaign GPS networks using the methods described in Serpelloni et al., JGR, 2013, which include 1) the phase data reduction (by means of the GAMIT/GLOBK software), 2) the combination of regional and global solutions (from MIT) and the realization of a global (i.e., IGb08) reference frame and 3) the time-series analysis. The final velocity field (Fig. 2) is obtained from the analysis of filtered time-series, where a continental-scale Common Mode Error has been estimated using a PCA approach (as in Serpelloni et al., JGR, 2013). The 3D velocity field of the Great Alpine Area (GAR) is part of a wider geodetic solution that includes data from ~3000 cGPS stations operating in the Euro-Mediterranean and African region. The figure shows horizontal velocities in a fixed Eurasian reference frame and the IGb08 vertical velocities.

corresponding authors: simone.salimbeni@ingv.it - enrico.serpelloni@ingv.it - silvia.pondrelli@ingv.it

THE SHEAR WAVE SPLITTING MEASUREMENTS

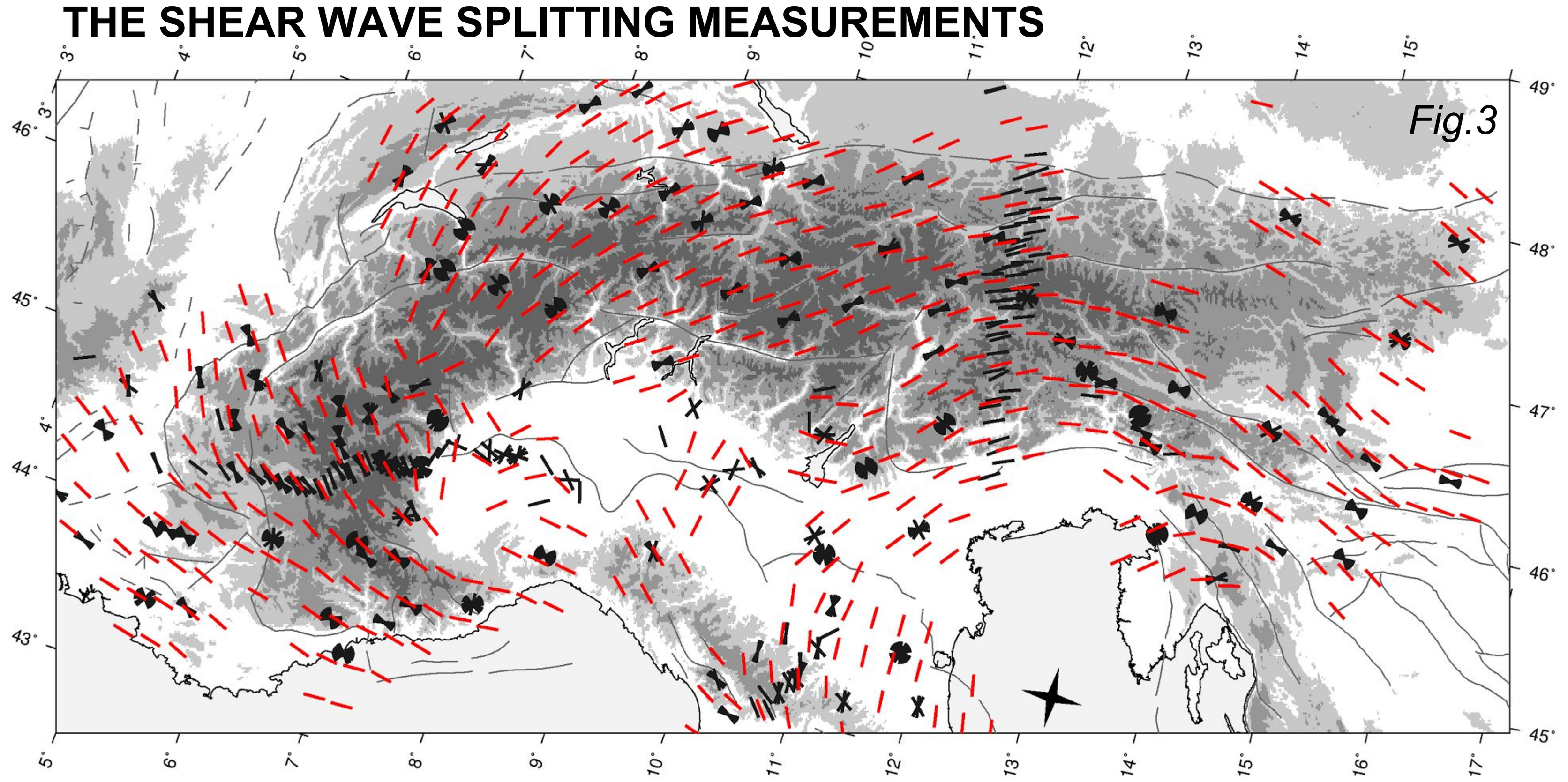

Map of the single SKS shear wave splitting measurements (in dark in Fig.3) extracted from SplitLab database (Wüstefeld et al., PEPI, 2009) and used to sketch the deformation in the Alpine upper mantle structure. In Western Alps and Po Plain region, SKS-splitting results of CIFALPS project are used (Salimbeni et al., in preparation; see poster EGU X2.207). Each segment is plotted in agreement with fast axes azimuth and scaled with the same delay time values.

To draw the continuous horizontal mantle deformation pattern, the initial dataset is purged of measurements with delay time values lower than 0.4 sec. and greater than 3.0 sec., and then interpolated with a smoothing algorithms (Müller et al., 2003, in Ameen (Ed), Geol. Soc. London Spec. Pubb. vol 209) over a regular grid of 0.25° X 0.25°. A tricubic weight power function is used over cells that, inside a searching radius of 40 Km, contain at least 5 SKS measurements. The result of interpolation is plotted using red bars.

THE GEODETIC STRAIN-RATE FIELD

We estimate the geodetic strain-rate field using the spherical wavelet-based method of Tape et al., GJI, (2009), which allows the estimation of a spatially continuous velocity field on a sphere starting from a set of irregularly spaced geodetic stations. The velocity value at a given point of the Earth's surface is obtained as a superposition of values obtained at different spatial scales. The multiscale aspect is achieved by using wavelets from progressively finer meshes, which goes to finer scales only where justifiable, based on the GPS site density, that is allowing for short-scale spherical wavelets in the estimation where GPS stations are dense, and allowing only for long-scale spherical wavelets in the estimation where stations are sparse. The method locally matches the smallest resolved process according to the local spatial density of observations. Using Tape's notation, q indicates wavelets order and a corresponding spatial scale. In case of tectonic deformation, reasonable maximum values of q ranges between 7 and 9, corresponding to scales of 55 and 14 km, respectively. The investigated area allows for minimum scale wavelets equal to 2 corresponding to a spatial scale of 1750 km. We test different maximum values of q (7≤q≤10). With q_{max} greater than 9 (q = 10, corresponding to a spatial scale of ~7 km) only, spot-like areas are resolved (Fig. 5). While the GPS network in the Italian Alps allows for a rather uniform value of q_{max} = 9 (corresponding to a spatial scale of ~14 km), over the GAR, geodetic strain rate is resolved at a spatial scale corresponding to a q_{max} = 8, that is the GPS network in the study area allows to resolve geodetic strain at a smaller spatial scale of 27 km. Fig. 4 shows the strain-rate field estimated using 2 ≤ q ≤ 8, where the colours show a scalar strain-rate value (the square root of the sum of squares of the strain-rate tensor components) and the black arrows shows the principal strain-rate axes.

Wavelets order	Spatial scale (km)
q = 2	1763.41
q = 3	881.71
q = 4	440.85
q = 5	220.43
q = 6	110.21
q = 7	55.11
q = 8	27.55
q = 9	13.78
q = 10	6.89
q = 11	3.44

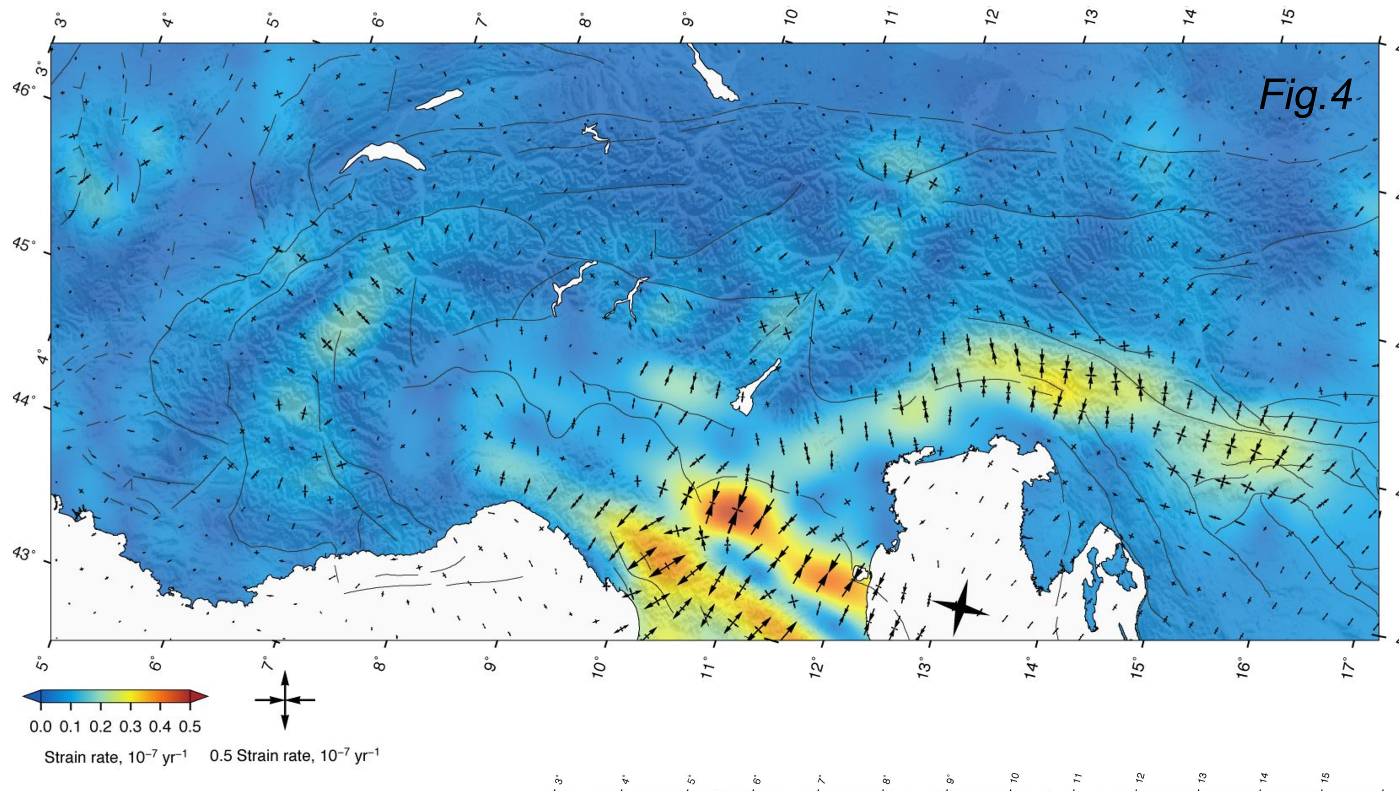

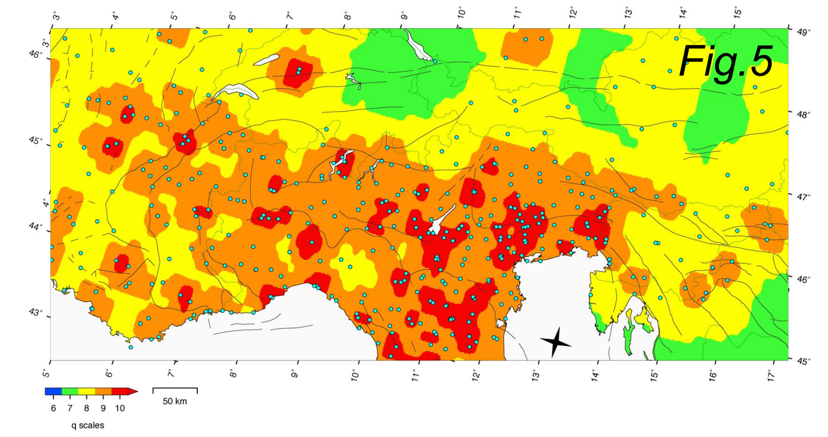

In our strain-rate analysis (Fig. 4) we consider the vertical component of the velocities (see Tape et al., GJI, 2009), but we found that the spatial gradients of the vertical velocity field doesn't constitute a significant part of the deformation over the Alps causing insignificant differences with respect to the strain-rate field obtained using the horizontal components.

Fig.s 6 and 7 show the continuous multi-scale q(2≤q≤8) horizontal and vertical velocity fields. In Fig. 6 the colours show the continuous speed in a fixed-Eurasian reference frame and the dashed red circles are the small circles around the geodetic pole of rotation (white star) showing the motion direction of Adria relative to Eurasia. In Fig. 7 red and blue colours represent positive (uplift) and negative (subsidence) vertical rates. The dashed lines show the contours of the filtered topography.

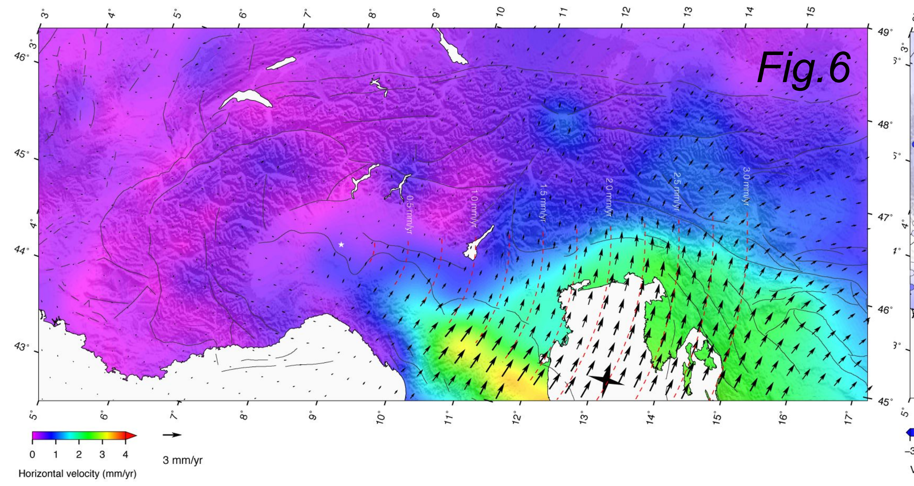

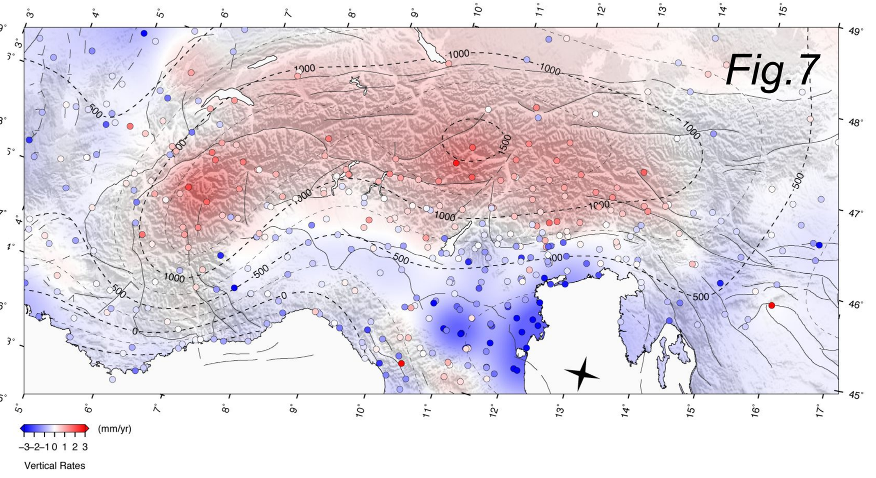

SEISMIC ANISOTROPY VS GEODETIC DEFORMATION

To investigate possible relationships between seismic anisotropy in the lithospheric mantle and the present-day surface deformation field, we determine the no-length-changes (NLC) orientations from our multi-scale geodetic strain-rate field. Within a three-dimensional strain rate field, in which the magnitude of shear strain rate (ε_{xy}) exceeds the magnitude of dilatational strain rate, there are two planes of shear. These two planes of shear (or directions of no length change in the velocity field) are analogous to the nodal planes of an earthquake focal mechanism. Holt and Haines (TECT., 1993) showed that at any given point in a strain rate field, the strike direction of these two planes of shear on the horizontal surface is defined by:

$$\tan\theta_f = \frac{-\dot{\varepsilon}_{xy} \pm \sqrt{\dot{\varepsilon}_{xy}^2 - \dot{\varepsilon}_{xx}\dot{\varepsilon}_{yy}}}{\dot{\varepsilon}_{yy}}$$

where ε_{xx} , ε_{yy} , and ε_{xy} are the three horizontal strain rate tensor components (x is positive to the east and y is positive to the north), and φ is the strike angle of the shear plane with respect to the x-axis direction. For strike directions that are equal, the faulting style corresponds to pure dip slip.
We exploit the multi-scale approach used in this work by comparing the directions of the seismic anisotropy (i.e., the smoothed values of Fig. 3) with the no-length-changes directions computed from strain-rate fields obtained using different intervals of wavelets orders, considering that the use of higher q_{max} values (>8) implies the inclusion in the final multi-scale strain-rate field of local deformation signals, likely not associated to tectonic and geodynamic processes. The use of lower values of q_{max}, on the contrary, results in a long-wavelength velocity and strain-rate fields, which can be assumed to be representative of larger-scale (geodynamics) processes, filtered by local and tectonic (crustal) deformation signals. Figures 8 and 9 shows two examples of geodetic strain-rate fields, with estimated NLC directions obtained by using q(2≤q≤6) and q(2≤q≤9) wavelets orders.

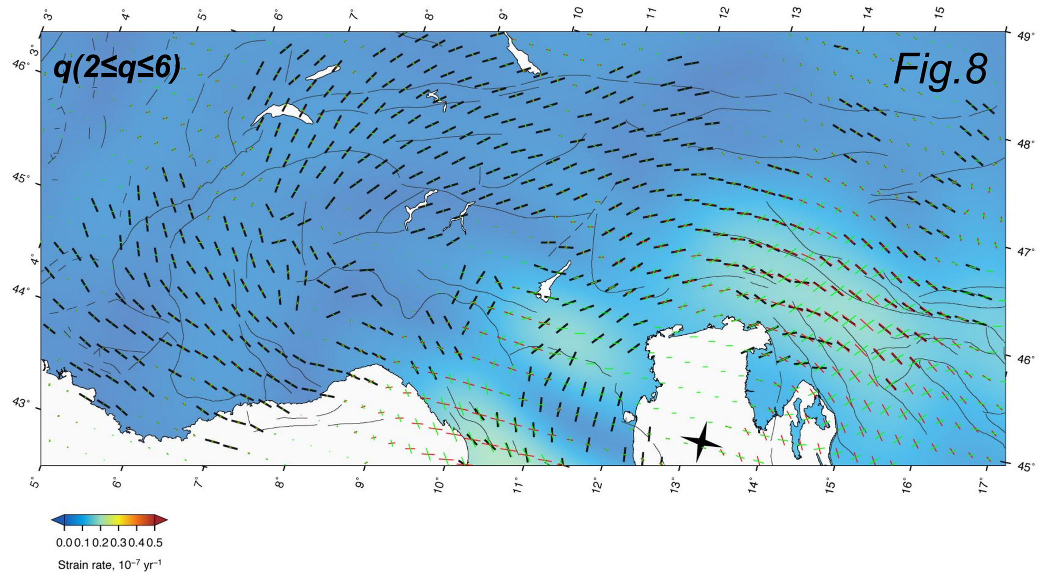

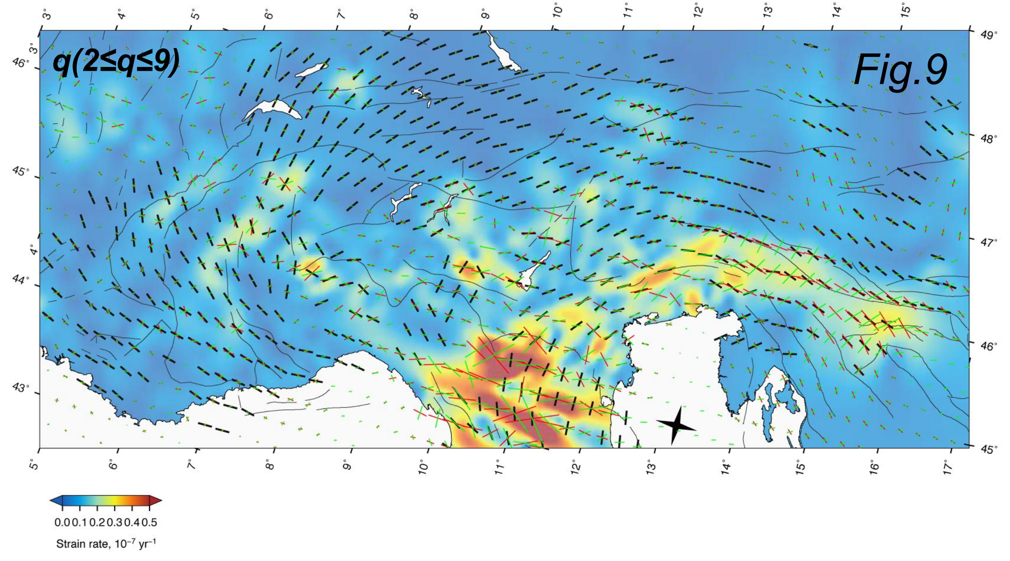

Fig.s 8 and 9 show the smoothed SKS directions (black bars) together with the directions of the dextral (red bars) and sinistral (green bars) planes of geodetic shear, plotted over a map of the multi-scale maximum shear rates. The length of the NLC symbols are scaled with respect to the shear rate values. Fig. 8 shows the results obtained using only low values of q (2≤q≤6), whereas Fig. 9 is obtained using a higher q_{max} = 9 (i.e., that accounts for short wavelength features of the geodetic deformation field), resulting in localized regions of higher deformation rates.

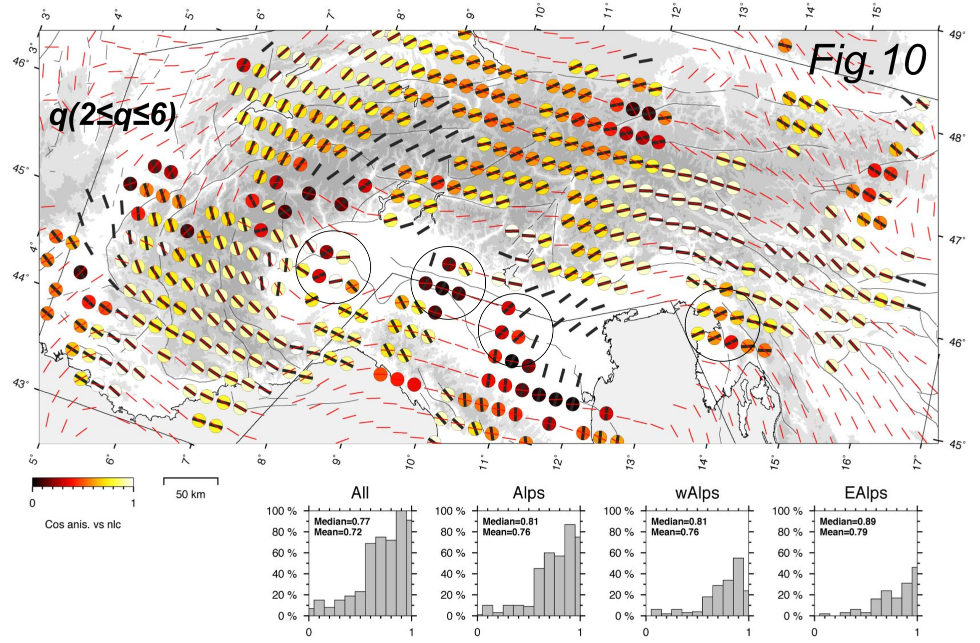

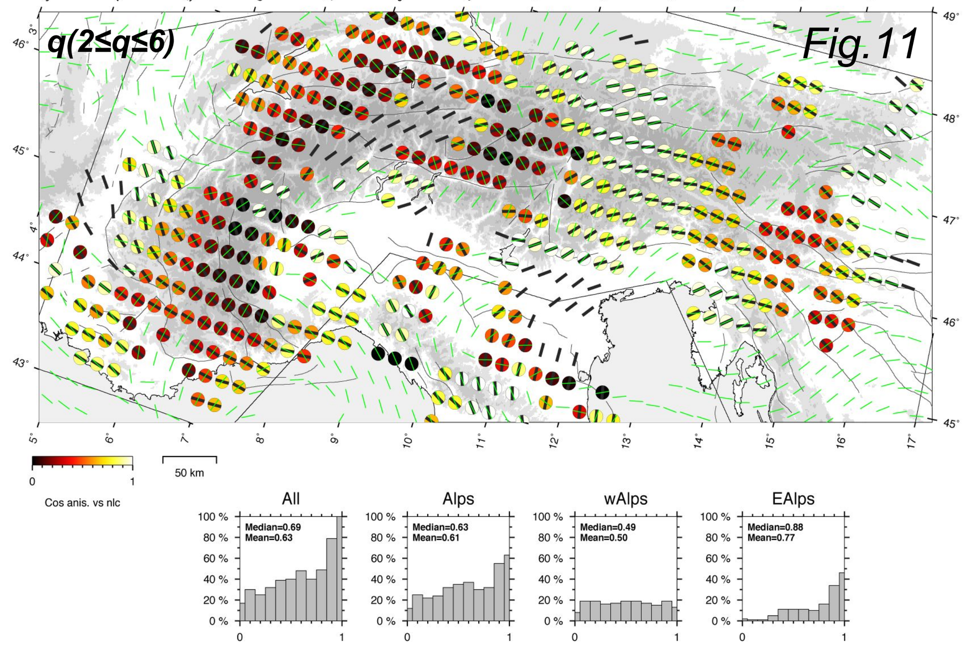

In order to quantitatively compare the geodetic NLC and seismic SKS directions we calculate the cosine of the angle measured between the directions of dextral (Fig. 10) and sinistral (Fig. 11) planes of shear and the smoothed SKS directions (Fig. 3). In Fig.s 10 and 11 this value is plotted with a color scale between 0 (black) and 1 (white), where dark colours indicate greater discrepancies between the two orientations while light colours indicate a better agreement.

We compared the SKS directions with the NLC directions estimated from the multi-scale strain-rate fields obtained using different intervals of wavelets orders. In particular using 2≤q≤5, 2≤q≤6, 2≤q≤7, 2≤q≤8, 2≤q≤9. We found a better agreement between orientations of mantle anisotropy and geodetic planes of shear using q_{max}<8, suggesting that filtering out the smaller wavelength tectonic signal improve the agreement between the deep and shallow deformation indicators.

We found that in all cases, i.e. for all of the wavelets orders considered in the multi-scale geodetic strain-rate analyses, the dextral NLC orientations better match the orientations of the seismic anisotropy. This observation is in agreement with the general eastward motion and right-lateral kinematics of the Alpine belt, as observed by GPS velocities and seismotectonic data.

In particular, we found a better agreement between geodetic and seismic observations in the eastern Alps, whereas the agreement is poorer in the western Alps.

By examining the differences between SKS and the geodetic NLC obtained from the strain-rate fields estimated using only the horizontal GPS velocities and including also the vertical velocities we found no significant differences, suggesting that the vertical velocity field doesn't constitute a significant part of the deformation over the Alps.

In all the cases, i.e. for all of the wavelets orders considered in the multi-scale geodetic strain-rate analyses, some regions show larger discrepancies between SKS and dextral planes of shear (see Fig. 10). For some of these areas (indicated in Fig. 10 with black circles) the reason is most likely due to the poorer seismic anisotropy measurements.